ARTICLE   OPEN

Large-area photonic lift-off process for flexible thin-film transistors

Adam M. Weidling[1], Vikram S. Turkani[2], Vahid Akhavan[2], Kurt A. Schroder[2✉] and Sarah L. Swisher [1✉]

Fabricating flexible electronics on plastic is often limited by the poor dimensional stability of polymer substrates. To mitigate, glass carriers are used during fabrication, but removing the plastic substrate from a carrier without damaging the electronics remains challenging. Here we utilize a large-area, high-throughput photonic lift-off (PLO) process to rapidly separate polymer films from rigid carriers. PLO uses a 150 µs pulse of broadband light from flashlamps to lift-off functional thin films from glass carrier substrates coated with a light absorber layer (LAL). Modeling indicates that the polymer/LAL interface reaches above 800 °C during PLO, but the top surface of the PI remains below 120 °C. An array of indium zinc oxide (IZO) thin-film transistors (TFTs) was fabricated on a polyimide substrate and photonically lifted off from the glass carrier. The TFT mobility was unchanged by PLO. The flexible TFTs were mechanically robust, with no reduction in mobility while flexed.

INTRODUCTION

As the complexity of flexible electronic devices such as flexible displays and sensors has increased, new plastic-compatible manufacturing methods are becoming necessary to produce high-yield, low-defect flexible circuits. While solution-processed methods such as printing can be used to fabricate circuits on low-temperature substrates[1], printing is not always a feasible option to realize complex, high-density circuits with small devices. In particular, high-resolution display applications typically require single-micron feature sizes[2,3] and excellent uniformity over large-area substrates. For these applications, more precise fabrication techniques such as photolithography are required. However, due to the poor dimensional stability of polymers, even low-temperature processes such as soft bakes during lithography can alter the substrate dimensions. As the feature size decreases, even micron-scale changes in the substrate dimensions can introduce errors in subsequent alignment steps[4,5]. One solution to this problem is transfer printing[6], in which materials are fabricated on one substrate and then transferred to a receiver substrate. However, transfer printing typically requires the use of an adhesion layer or careful modification of the substrate surface to facilitate ink transfer[6]. Alternatively, the problem of dimensional stability can be overcome by attaching the polymer film to a rigid carrier during device fabrication, then releasing the polymer substrate with the fully fabricated device layer on top. For this reason, the separation of polymer films from rigid carriers remains a crucial step in creating next-generation flexible electronics.

A variety of methods have been investigated to release a plastic substrate from a rigid carrier. Laser lift-off (LLO) utilizing excimer lasers has long been the method used in industry to delaminate polymer films from the rigid carriers that are required during electronics fabrication[7–17]. The mechanism of lift-off is based on the selective ablation of the polymer film at the interface between the polymer and the rigid carrier. The interaction between polymers and lasers has been extensively studied[18–26], and these studies led to the LLO technique. In LLO, the laser is scanned across the back of the glass substrate and ablation is achieved by

absorption occurring in the polymer substrate itself, as polymers typically absorb wavelengths in the ultraviolet (UV) region of the spectrum. The absorbed laser energy heats the polymer and causes ablation at the glass/polymer interface. Excimer LLO has several attractive properties such as the ability to maintain local radiation and achieve low global temperatures[17]. However, expensive laser systems are required, and the lift-off process is sensitive to variations in the laser parameters. Power fluctuations and nonuniform rastering of the laser system can cause defects and reduce yield[14]. LLO is also a time-intensive rastering process, which translates to higher production costs when working on large-area substrates[27].

To overcome the challenges of LLO, alternative delamination techniques have been investigated. Temporary bonding layers such as tapes and adhesives have been used to attach the plastic film to the carrier during fabrication, but even some of the bonding materials themselves produce small dimensional changes[28–33]. Many also require UV or thermal energy[30,34–37], solvents[34], or mechanical force to delaminate the sample[30,38–40]. Inorganic separation layers such as oxidized tungsten are more stable than adhesives at high processing temperatures, but still require substantial delamination force[41]. Thermal ablation from joule heating has also been demonstrated[42], but is not widely used.

In this study, we utilize a non-laser photonic lift-off (PLO) process to overcome the challenges presented by the previous techniques used to separate polymer films from rigid carriers. PLO uses broadband light (200–1100 nm) from a flashlamp to lift-off a polymer film from a rigid carrier coated with a light-absorbing layer (LAL), where the polymer film may contain functional devices[43]. Preliminary results using flashlamps instead of lasers for polymer lift-off were reported recently[44,45], but no active devices or TFTs were included. Compared to those results, PLO in this work utilizes a simple single-layer metal absorber rather than a four-layer structure, and an ultra-fast pulse duration that is only 2–5% of the previously reported pulse length. Flexible nanocrystal photovoltaic devices were recently demonstrated using PLO[46]. Compared to a raster process such as LLO, the PLO process is

[1]Department of Electrical and Computer Engineering, University of Minnesota Twin Cities, 4-174 Keller Hall, 200 Union Street S.E., Minneapolis, MN 55455, USA. [2]NovaCentrix, 400 Parker Drive, Suite 1110, Austin, TX 78728, USA. ✉email: kurt.schroder@novacentrix.com; sswisher@umn.edu
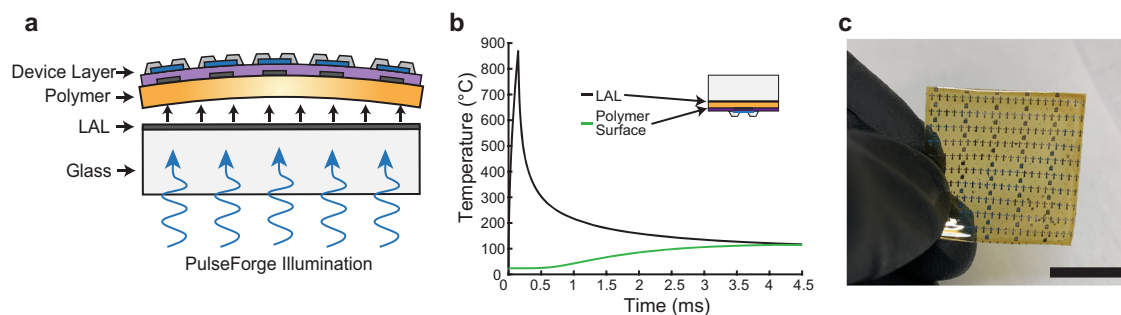
Fig. 1 Photonic lift-off of a polymer substrate containing thin-film devices from a glass carrier. a Typical material stack for the photonic lift-off (PLO) process, showing illumination through the glass to the light absorber layer (LAL). **b** Simulated thermal response during PLO at the polymer/LAL interface and on the surface of the polyimide where the device layer would reside. **c** Flexible TFT array on polyimide lifted off using PLO. Scale bar: 10 mm.

advantageous as it can enable large-area lift-off (150 mm × 75 mm) in one flash of light lasting between 100–200 µs, thus enabling higher throughput. Furthermore, the presence of the LAL prevents direct illumination of the polymer substrate during lift-off and facilitates cleaner lift-off without polymer ashing, which is a common concern with LLO. The presence of the LAL makes PLO a polymer-agnostic process enabling the lift-off of a wide range of polymers.

Here we report the fabrication of flexible thin-film transistors (TFTs) using PLO. Polyimide with a low coefficient of thermal expansion (CTE) was used to minimize residual film stress. Indium zinc oxide (IZO) TFTs were fabricated on the polyimide films and subsequently released from the carrier using PLO. The released devices demonstrated no significant changes after the PLO process, yielding mobility of ~3 cm^2 V^{-1} s^{-1} before and after lift-off. The flexible TFTs were robust to bending stress, showing no notable decrease in mobility while bent with a 10 mm radius of curvature. When combined with the ability to successfully separate the PI from the carrier, the low-CTE PI creates a robust fabrication platform for flexible electronics that allows conventional patterning and deposition techniques to be used on a plastic substrate while maintaining dimensional stability up to 380 °C. A 3D finite element model was developed to validate the thermal response in the substrate during lift-off. The modeled temperature in the polyimide film reaches 865 °C at the ablation layer but stays below 120 °C at the device layer, which is low enough to avoid damage or induce chemical changes in the thin-film transistors. The model shows that the maximum temperature at the device layer during PLO is strongly impacted by the thickness and material properties of the polymer film, highlighting the value of the model to guide PLO device design. This work demonstrates the feasibility of PLO to successfully release polyimide substrates containing flexible electronic devices from glass carriers after withstanding conventional lithographic processing methods.

RESULTS AND DISCUSSION
Photonic lift-off process

Figure 1a shows a typical material stack used in PLO to lift-off a polymer carrying electronic devices. First, a glass carrier substrate is coated with a thin metal light absorber layer (LAL), typically 250 nm of sputtered TiW (10:90). A polymer coating is then applied to the LAL, and finally, the electronic structures are fabricated on the surface of the polymer film. The PLO process involves irradiating the LAL through the glass with a broadband (200–1100 nm) light pulse using the PulseForge photonic curing system (Fig. 1a). The PulseForge generates an intense pulse of light (output up to 45 kW cm^{-2}) with a 150 µs pulse length, providing adequate heating over a short time period to lift-off the

polymer. The primary mechanism of photonic lift-off is thermal decomposition of the polymer at the LAL/polymer interface due to the high temperature achieved at the LAL. Figure 1b shows the simulated thermal response of the LAL during the PLO process, illustrating that the temperature at the LAL exceeds 850 °C in less than 0.5 ms, but the top surface of the polyimide stays below 120 °C. A flexible array of TFTs on a polyimide substrate that was delaminated using photonic lift-off is shown in Fig. 1c.

The metal LAL is the key enabler of the PLO process. Its primary purpose is to convert the absorbed optical energy into the thermal energy needed to facilitate the ablation of the polymer (e.g., polyimide) at the metal interface, enabling lift-off of the polymer film from the rigid carrier. Its secondary purpose is to block the transmission of broadband light into the polymer and device layers. Thus, the design requirements for the LAL are that the optical transmittance should be nearly zero and the reflectance should be minimized, and the absorbance maximized. Not only are the optical parameters important, but the adhesion between the LAL and the glass is also crucial. The metal must also have sufficient thermal stability to withstand high temperatures without cracking. In general, these design guidelines are similar to those we have previously discussed for photonic curing of IZO-based TFTs[47]. In this work, we utilized TiW (10:90) for the LAL due to its strong adhesion to the glass, high optical absorption, and thermal robustness. The metallic LAL was not cracked or otherwise damaged during PLO, and the metal-coated glass substrate can be re-used for multiple PLO runs (Supplementary Fig. 1 and Supplementary Discussion). The coefficient of thermal expansion also closely matches that of the glass substrate (4–4.5 ppm °C^{-1} and 3.2 ppm °C^{-1}, respectively). Furthermore, it was observed that cleaning the glass prior to deposition of the absorber layer was an important factor in the overall success of PLO. If improperly cleaned, the adhesion between the LAL and the glass can be a failure point causing the metal to delaminate during PLO.

The optical properties of the LAL were characterized using UV-Vis spectroscopy to determine its spectral absorbance. Using an integrating sphere, the reflectance and transmittance were measured, and the absorbance was calculated ($A = 100 - T - R$). Optical measurements (Fig. 2) with light incident on the back of the glass substrate reveal that the absorber layer coating has ≈0% transmission throughout the mid-UV to the near-IR region, as desired. These measurements also confirm the high absorbance in the TiW LAL, which is essential for efficient heating[47]. The absorbance of the LAL is >55% in the wavelength range corresponding to the dominant emission from the PulseForge lamp ($\lambda = 400$–600 nm, Supplementary Fig. 2), providing sufficient absorption in the LAL for photonic lift-off.

Because the LAL protects the polymer layer from direct illumination, it makes the PLO a polymer-agnostic process. To demonstrate this, a variety of both thermoset and thermoplastic
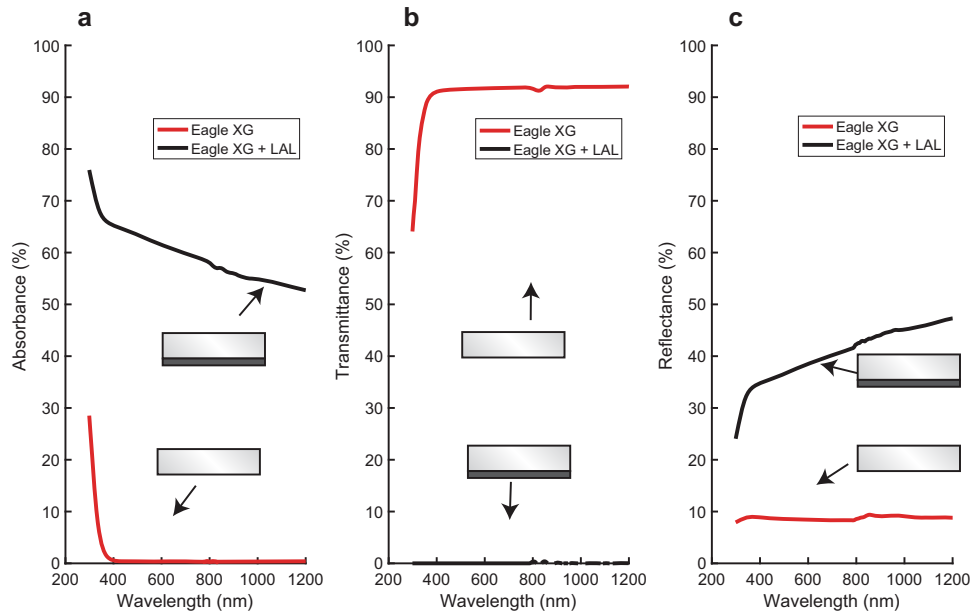
Fig. 2 UV-Visible spectroscopy of glass carriers with and without light absorber layer. a Absorbance, **b** transmittance, and **c** reflectance spectra for Eagle XG glass with and without the 250 nm TiW light absorber layer (LAL).

Table 1. Material parameters used to create a 3D model of the thermal response during photonic lift-off.

Material	Density (g cm^{-3})	Heat capacity (J kg^{-1} C^{-1})	Thermal conductivity (Wm^{-1} K^{-1})
TiW	19.25	134	160
Eagle XG	3.28	1100	1.2
Polyimide (PI 2611)	1.4	1009	0.12

polymers were lifted off from the LAL-coated glass carrier using the PLO process. Supplementary Fig. 3 shows successful PLO of a thermoset polymer such as polyimide (PI 2525 HD Microsystems), clear polyimide (KOLON CPI™), and a thermoplastic polymer such as polyurethane (Lubrizol Sancure™ 1511). The processing conditions were adjusted to account for the decomposition temperature of each polymer (Supplementary Table 1 and Supplementary Discussion).

Finite element modeling (FEM)
The PLO process involves converting the incident optical energy on the LAL into thermal energy to ablate a polymer. Thus, it is imperative to study the thermal response at the LAL-polymer interface during photonic lift-off. To estimate the thermal response, a 3D finite element analysis model for the PLO process was developed using COMSOL® Multiphysics. The geometry in the model was defined to match the stack used in this process (700 µm Eagle XG glass, 250 nm TiW, and 30 µm PI). The 3D heat conduction equation used to solve for the thermal gradients is shown in Eq. 1.

$$\rho c_p \frac{\partial T}{\partial t} + \nabla \cdot \mathbf{q} = 0 \qquad (1)$$

Here ρ is the material density, c_p is the specific heat capacity, T is the temperature, $q = -\kappa \nabla T$ is the local heat flux density, and κ is the thermal conductivity. The density, heat capacity, and thermal conductivities used in the simulation are shown in Table 1.

The heat flux incident on the LAL was modeled using the deposited beam power physics module in COMSOL Multiphysics.

The energy incident on the LAL was determined by measuring the radiant exposure of the lamp irradiating at typical lift-off conditions (950 V and 150 µs) on the bolometer, through the Eagle XG glass (Supplementary Fig. 4). The bolometer recorded an average radiant exposure of 3.26 ± 0.05 J cm^{-2}. For comparison, the radiant exposure measured directly by the bolometer (without the glass) was 4.51 ± 0.1 J cm^{-2}. The radiant exposure measured through the glass was multiplied by the absorbance of the LAL obtained from UV-Vis spectroscopy. The product represents the energy absorbed in the LAL, which was 1.98 J cm^{-2}.

Convective heat flux was defined at all boundaries using a convective heat transfer coefficient of 15 Wm^{-1} K^{-1} to model the interaction of the sample with air because the sample is typically suspended during the PLO process. A time-dependent solution to Eq. 1 was obtained and the resulting thermal profiles as a function of time are shown in Fig. 3. Figure 3a shows temperature as a function of depth where 0 µm is the top surface of the PI where the thin-film electronics would reside, and 30 µm is the LAL-PI interface. From 30 to 730 µm is the bulk of the glass carrier. Note that the depth axis in Fig. 3a has been truncated at 300 µm because beyond that point the glass remains at room temperature. The maximum temperature of 865 °C is achieved at the LAL-PI interface at 150 µs, which corresponds to the end of the PLO light pulse. It is important to note that the surface of the PI where the devices are fabricated does not see this exceedingly high temperature. As time progresses, since the thermal conductivity of the glass (1.2 Wm^{-1} K^{-1}) is higher than that of the PI (0.12 Wm^{-1} K^{-1}), the heat conducts into the glass first whereas the heat conduction into PI is slower. Figure 3b shows the thermal gradient through a cross-section of the entire device stack at various time intervals, demonstrating that the heat is confined to a very thin region to ablate the PI and that the temperature rapidly drops below the maximum working temperature of the PI. The simulation shows that the maximum temperature obtained at the surface of the PI during lift-off is 118 °C. In reality, after the peak temperature is reached, the polyimide is no longer in perfect contact with the LAL due to the ablation, so we hypothesize that this simulation is an overestimate and that the actual temperature at the surface of the PI is lower. In this way, the PLO process is self-limiting. The temperature obtained on the surface of the PI is well within the operating limits of standard polyimide films and is no
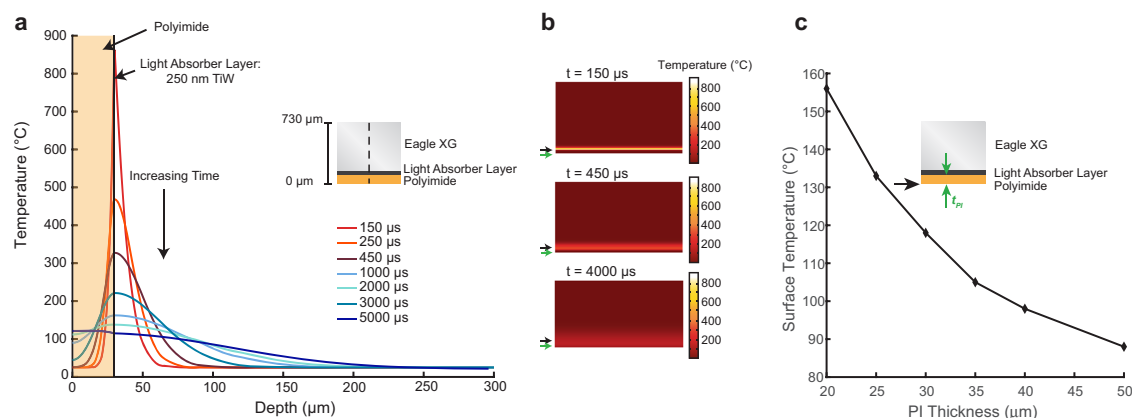
Fig. 3 **Modeled thermal response during photonic lift-off of polyimide from glass carrier. a** Thermal response as a function of depth at various time intervals. The depth plots were truncated at 300 μm into the glass because no temperature rise was present beyond that point. **b** Heatmaps showing the temperature gradient across the entire 730 μm stack depth at three time points, where the black and green arrows indicate the position of the LAL and the top surface of the polyimide, respectively. The maximum temperature is reached at $t = 150$ μs, and the sample reaches thermal equilibrium around $t = 4000$ μs. **c** Simulated peak temperature at the surface of the polyimide (PI) as a function of the thickness of the PI layer for a 950 V, 150 μs photonic lift-off pulse. The inset shows the Eagle XG/TiW/PI material stack, with green arrows indicating the thickness of the PI layer and a black arrow indicating that the simulated temperature refers to the top surface of the polyimide.

higher than a typical soft bake temperature during lithography. Based on these results, the PLO process is not expected to damage electronic devices on the surface of the polyimide.

The low thermal conductivity of the PI ensures that the heat conduction to the top surface is minimized. However, as the PI thickness decreases, the heat does not have to penetrate as far to reach the devices, and the temperature experienced on the device surface of the PI increases. The peak temperature at the surface of the PI was simulated using a 950 V, 150 μs pulse using the same structure as shown in Fig. 3a, but with the PI film thicknesses ranging from 20 to 50 μm. As the film thickness increased, the peak temperature on the device surface of the PI decreased from 155 to 88 °C (Fig. 3c). This shows that the temperature on the PI surface is inversely related to the PI thickness. Thus, the resulting heat transfer to the devices depends on the polymer thickness and its thermal conductivity.

Photonic lift-off of TFTs on PI

Indium zinc oxide TFTs fabricated on a 30 μm thick polyimide layer (PI 2611) were subjected to the PLO process to separate the polyimide substrate from the LAL-coated glass carrier. PI 2611 is a low-CTE version of polyimide, which was important to minimize residual film stress after PLO. The sample was face down and suspended on glass microscope slides during the PLO process, such that the light passes through the glass carrier and is incident on LAL. Suspending the sample ensures that the active layer does not contact the platen and damage the thin-film devices. The released PI film containing flexible IZO TFTs is shown in Fig. 4.

During PLO, the temperature in the LAL must exceed the decomposition temperature of the polymer to successfully achieve lift-off. The PLO process condition was optimized by varying the pulse duration from 130 to 160 μs at a fixed capacitor bank voltage of 950 V, where longer pulses lead to higher incident exposure and result in higher temperatures. Figure 5a shows the LAL-coated glass carrier and the PI substrates lifted off with varying pulse durations. Pulse duration and capacitor bank voltage are the two primary process variables in the PulseForge photonic curing tool, collectively contributing towards the energy density and incident power output of the system. Energy densities obtained as a result of varying pulse duration were correlated to the modeled maximum temperature at the LAL-PI interface (Fig. 5b). The samples were successfully lifted off when the pulse duration was below 140 μs, but the released devices exhibited a

large degree of PI curling, which indicates residual stress in the PI. These PI samples required a relatively higher peel force to separate them from the carrier after the PLO. This increase in the peel force indicates some residual adhesion between the PI and the carrier was still present after PLO. Devices lifted off with pulse lengths greater than 140 μs exhibited less curling and laid flat once released. Although the specified decomposition temperature of PI 2611 is 620 °C, we found it advantageous to use PLO pulses of at least 140 μs (corresponding to a peak temperature of ~750 °C) to ensure easy release from the carrier. We did not notice any soot formation on the LAL in any of these devices, which has been observed in previous studies[44]. As the pulse width increases the resulting temperature at the surface of the PI is likely to increase. Especially in thin PI films, this can result in damage to the devices, so pulse durations should be kept as short as possible without inducing curling or sacrificing lift-off yield.

TFT characterization

The IZO TFTs were characterized before and after the PI was released from the glass carrier using PLO. The TFT transfer and output curves were measured (Fig. 6), and device metrics such as mobility, subthreshold slope, and leakage current were extracted. Prior to PLO while the polyimide was still attached to the glass carrier, these devices demonstrated average field-effect mobility of 3.15 cm^2 V^{-1} s^{-1}, a subthreshold slope of 152 mV per decade, and had very low gate leakage. After being released from the rigid carrier using PLO, the on-current decreased by 7%, but otherwise, the device characteristics showed no appreciable change. The flexible IZO TFTs had average field-effect mobility of 3.15 cm^2 V^{-1} s^{-1} and a subthreshold slope of 152 mV per decade. Importantly, the relatively small change in device characteristics after PLO indicates that the devices did not undergo any changes. This validates the claim that the bulk polyimide remains relatively unheated during PLO.

After PLO, the mechanical durability of the flexible devices was evaluated by measuring the TFTs while bent to either a 30, 20, or 10 mm radius of curvature. Devices were bent such that the bending axis was parallel to the channel width, placing the channel under tensile stress. Transfer and output curves measured while the devices were bent are shown in Fig. 7 and a summary of device performance is provided in Table 2. Overall, bending produced very little change in the device performance. Devices that were measured while bent to a 30 or 20 mm radius of
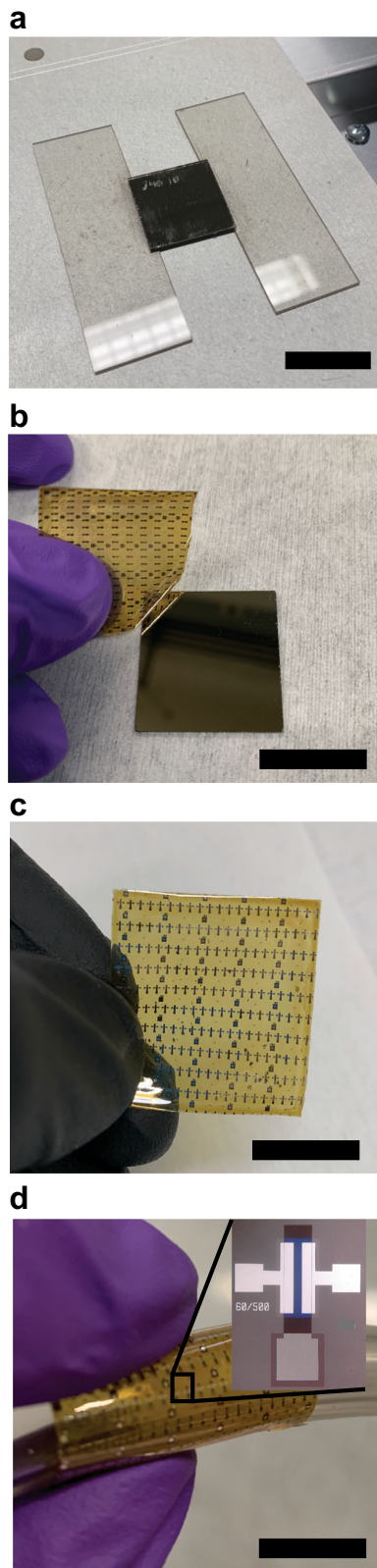
a Device suspended on glass slides before PLO.

Fig. 4 Photonic lift-off of IZO TFTs. a Device suspended on glass slides before PLO. Scale bar: 25 mm. **b** Device being removed from the LAL after PLO. **c** Flexible TFTs on polyimide after release from the carrier substrate. **d** Device bent around a plastic tube and inset showing a W/L = 500/60 μm device on polyimide. Scale bar in panels **b**–**d**: 10 mm.
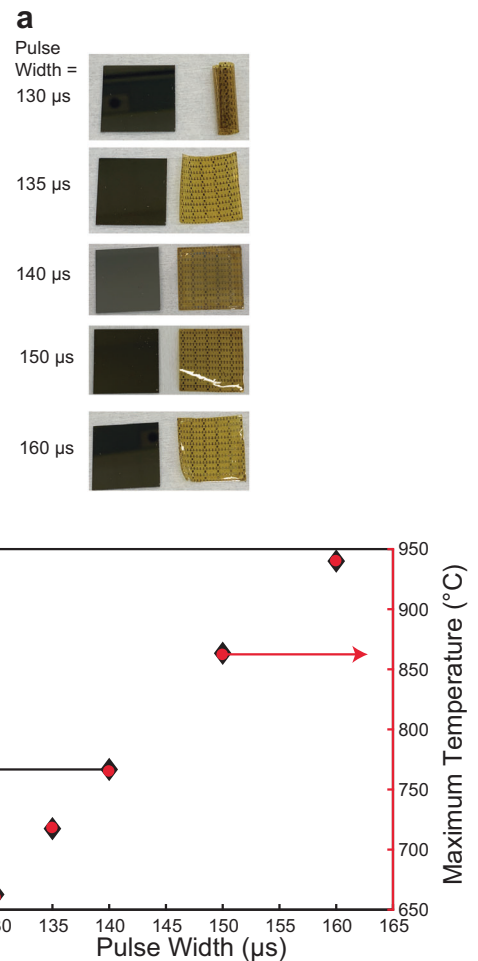

Fig. 5 Effect of pulse duration on the photonic lift-off process. a Released samples that underwent PLO at 950 V with illumination pulse widths ranging from 130 to 160 μs. **b** Energy incident on the LAL and the maximum simulated LAL temperature for different pulse widths.

curvature (Fig. 7a, d, b, e) have similar performance to both the rigid (unreleased) device and the released flat device, having mobility values of 3.13 cm^2 V^{-1} s^{-1} and low gate leakage. The devices measured with a bending radius of 10 mm (Fig. 7c, f) demonstrated a slight reduction in the linear hysteresis and an increase in leakage current. The subthreshold swing value slightly increased from 152 mV per decade to around 170 mV per decade when bending radii of 20 and 10 mm were used. This may indicate the formation of defects at the dielectric interface when the sample undergoes bending.

Process scalability

In this work, the PLO process was successfully used to lift-off PI films with IZO TFTs fabricated using 25.4 mm × 25.4 mm Eagle XG glass substrates as the rigid carriers. However, this PulseForge process can also be used to lift-off polymeric films from much larger carriers in a matter of seconds. The equipment used here has a single lamp with an irradiation area of 75 mm × 150 mm per flash. The same equipment can irradiate an area of 150 mm × 300 mm when a synchronized flash rate is combined with a motorized table to uniformly process a larger panel. Using proprietary lamp concatenation technology, production versions of this equipment having multiple lamps can irradiate an area of
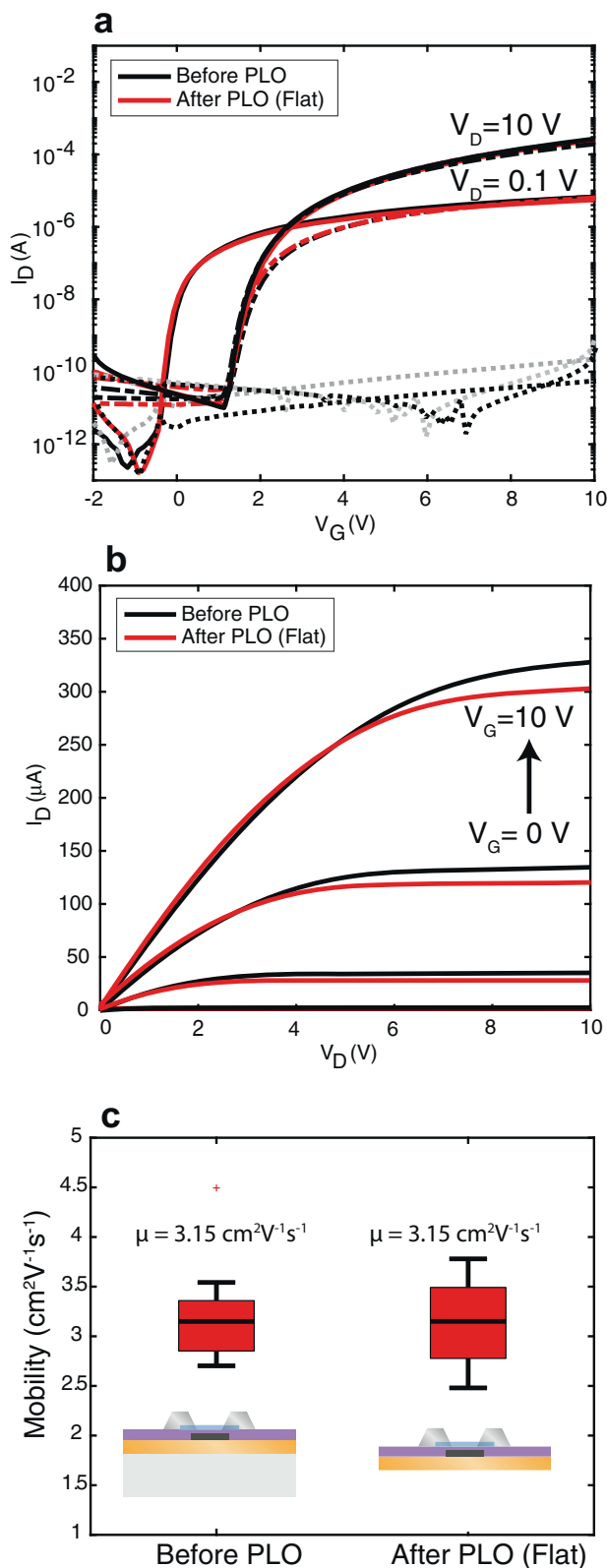
Fig. 6 Performance of IZO TFTs before and after photonic lift-off. **a** I_D-V_G transfer curves for IZO TFTs before PLO and after PLO. Solid lines are the forward sweep and dashed lines are the reverse sweep. **b** I_D-V_D output curves for devices before PLO and after PLO. **c** Mobility statistics for IZO TFTs before and after PLO. In the box and whisker plots, the centerline is the median, the box limits are the upper and lower quartiles, the whiskers are 1.5x the interquartile range, and the points are outliers.

150 mm × 75n mm per flash, where "n" is the number of lamps present. For example, a two-lamp production tool can lift-off a 150 mm × 150 mm substrate in one flash. A production version of this equipment with five lamps and a 375 mm processing width is shown in Supplementary Fig. 5. This five-lamp tool was used to demonstrate PI lift-off from a "Gen 2" glass carrier (365 mm × 465 mm, Fig. 8a), which was accomplished using a series of four flashes over 4 s. The large-area uniformity of the illumination from these tools is a critical capability that enables PLO to use multiple flashes and multiple passes to achieve rapid, high-yield lift-off. The modeled normalized illumination intensity of the five-lamp tool for a single flash (375 mm × 150 mm) obtained using a 3D ray-trace simulation is shown in Fig. 8b, with horizontal and lateral uniformity intensity profiles plotted in Fig. 8c. As seen in Fig. 8b, the processing area is uniformly illuminated, with less than 5% variability in illumination intensity over the central region. Using the motorized table and synchronized flashing in this manner, we estimated that a polymer film could be lifted off from a 1.5 m × 1.8 m "Gen 6" glass substrate in only ~40 s using three passes with a tool containing eight lamps (Supplementary Table 2). These results demonstrate that photonic lift-off is a highly scalable and industrially relevant process that can provide efficient, high-throughput polymer lift-off from glass carriers.

In conclusion, we have demonstrated the fabrication of flexible IZO TFTs on low-CTE polyimide films using photonic lift-off. The TFTs were fabricated using sol-gel IZO and microfabrication techniques (sputtering, lithographic patterning, a wet/dry etching) on a glass carrier substrate coated with a TiW light absorber layer. The PLO process was completed using a single 950 V 150 µs pulse from a flashlamp, which cleanly ablated the PI film from the surface of the light absorber layer and enabled the PI film containing a TFT array to be successfully lifted off from the LAL. The thermal response as a function of both time and depth into the material stack during PLO were verified with a 3D finite element model, indicating that the PI/LAL interface is heated to 865 °C while the surface of the PI containing TFTs does not reach temperatures greater than 118 °C. The TFTs were characterized both before and after PLO, showing that they experienced a negligible change in performance after lift-off from the glass substrate and even maintained a constant performance under bending. These TFTs mimic circuitry such as the backplane of a display, thus demonstrating that PLO is compatible with functional thin-film flexible electronics. The metal light absorber layer allows PLO to be used with a variety of polymer substrates, and the large-area uniformity means it is highly scalable to rapidly release polymer films from substrates over "Gen 2" (365 mm × 465 mm) dimension. Photonic lift-off is a robust fabrication platform that can solve many of the dimensional stability issues encountered with polymer substrates and enable high-density flexible electronics.

METHODS
Light absorber layer deposition
Before depositing the light absorber layer, the starting glass substrate (typically 25.4 mm by 25.4 mm Eagle XG display glass, Corning) was cleaned in a piranha bath consisting of four parts sulfuric acid and one part hydrogen peroxide. After this, a 250 nm TiW lift-off layer was deposited using magnetron sputtering with the sample platen heated to 250 °C. The sputtering power was 250 W under 5 sccm of argon. This resulted in a deposition rate of 12.2 nm per minute. The light absorber must be sufficiently thick to maximize absorption such that none of the incident optical energy is transmitted into the polyimide film.

Polyimide film formation
The PI film was obtained by spin coating PI 2611 (HD Microsystems) over the LAL. An adhesion promoter (VM-651) was used to ensure good adhesion between the metal LAL and the polyimide, which makes the PI
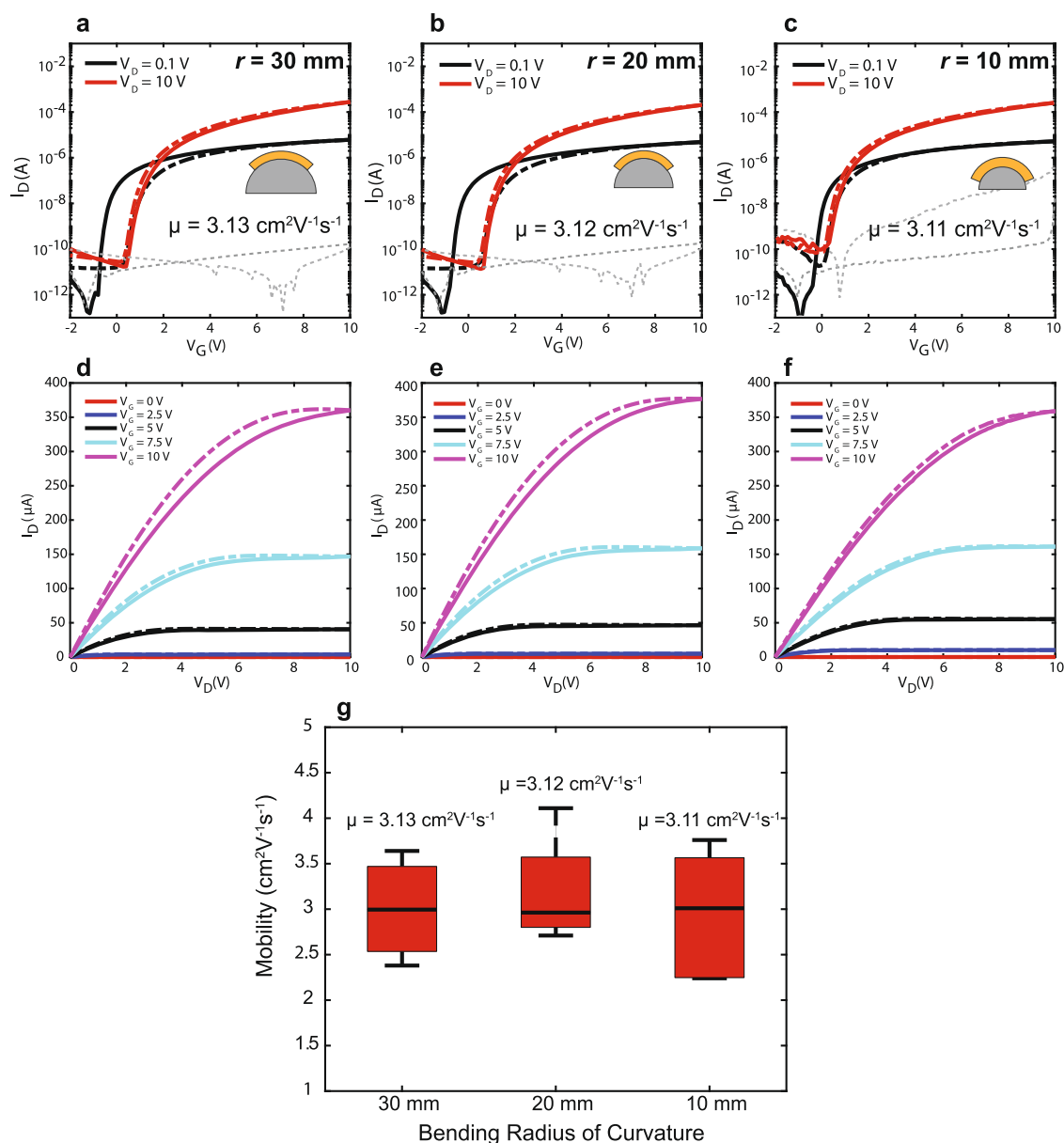
Fig. 7 Performance of flexible IZO TFTs under various bending radii. a, d Transfer and output curves for IZO TFTs while bent to a 30 mm radius of curvature. Solid lines are the forward sweep and dashed lines are the reverse sweep. **b, e** 20 mm radius of curvature. **c, f** 10 mm radius of curvature. **g** Mobility statistics for devices for various bending radii. In the box and whisker plots, the centerline is the median, the box limits are the upper and lower quartiles, the whiskers are 1.5x the interquartile range, and the points are outliers.

Table 2. Summary of IZO TFT characteristics before and after PLO, and while bent to a radius of curvature of 30, 20, or 10 mm.

Condition	Mobility ($cm^2 V^{-1} s^{-1}$)	Saturation hysteresis (mV)	SS (mv/dec)	Gate leakage (A)
Before PLO	3.2	130	152	$<10^{-10}$
After PLO (Flat)	3.15	120	152	$<10^{-10}$
$r = 30$ mm	3.0	120	152	$<10^{-10}$
$r = 20$ mm	2.96	130	170	$<10^{-10}$
$r = 10$ mm	3.01	120	170	$<10^{-7}$

2611 film thickness predictable and uniform. The adhesion promoter was diluted to a 1:500 ratio of VM-651: DI water and thoroughly stirred prior to spinning. The adhesion promoter was statically dispensed onto the absorber layer ensuring the entire surface was covered and was then allowed to stand for 20 s prior to spinning. The sample was spun at 3000 RPM for 40 s.

The polyimide precursor (PI 2611, HD Microsystems) was then applied. Prior to spinning the polyimide, it is crucial to ensure that the bottle is brought up to room temperature prior to opening it to avoid residual moisture. If the polyimide is poured into a secondary container for dispensing it must also be degassed to remove any air bubbles. The polyimide precursor was statically dispensed onto the center of the substrate (covering ~60%) and allowed to spread for 20 s. The sample was then spun at 500 RPM for 5 s to ensure sufficient spreading over the substrate and to allow excess PI to spin-off. The sample was then slowly
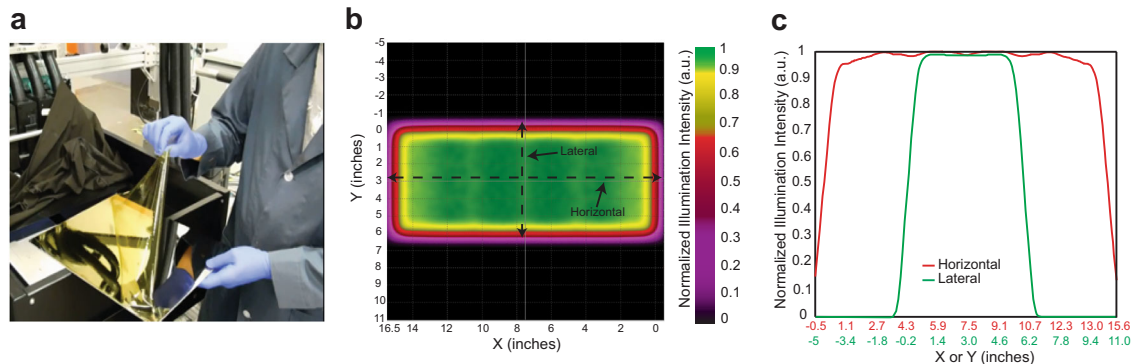
Fig. 8 Scalability of photonic lift-off. a Photonic lift-off of polyimide from a 365 mm × 465 mm Gen 2 glass carrier. **b** Normalized illumination intensity over a single flash area from a 5-lamp PulseForge photonic lift-off tool. **c** Normalized illumination intensity along the horizontal and lateral profiles indicated in panel **b**.

ramped up to 2100 RPM (over 10 s) where it was held for 35 s. After spinning, the sample underwent a three-step baking process consisting of 2 min at 120 °C, 2 min at 150 °C, and 5 min at 180 °C ensuring that solvents were removed. Three separate hotplates were preheated to the specified temperatures, and the sample was transferred between hotplates to avoid the need to ramp up to each setpoint. This spinning and baking step was repeated two more times yielding a three-layer polyimide film. The sample was then cured in a Sentro Tech programmable tube furnace. The cure consisted of a slow ramp (4 °C per minute) from 25 to 240 °C where it was allowed to dwell for 1 h. Then the sample was ramped from 240 at 2 °C per minute to 380 °C where it dwelled for 2 h. During the ramp from 240 to 380 °C, flowing nitrogen was introduced into the tube. Slow ramp rates are required to avoid rapid degassing a bubble formation in the film. After curing, the sample was then allowed to slowly return to room temperature. This process yielded a polyimide film that was ~30 μm thick with a surface roughness of 0.5 nm$_{RMS}$ (Supplementary Fig. 6 and Supplementary Discussion). If there is a significant amount of residual backside contamination from the adhesion promoter and PI, the backside should be cleaned prior to lift-off to prevent PI on the backside from absorbing the incident light pulse and decreasing energy transfer to the LAL.

Thin-film transistor fabrication

Bottom gate TFTs structures were fabricated onto the cured polyimide film. A 150 nm molybdenum gate electrode was deposited by DC magnetron sputtering and subsequently patterned using lift-off. The dielectric layer was 42 nm of HfO$_2$ deposited using plasma-enhanced atomic layer deposition (PEALD) at 100 °C. During the PEALD process, the back of the sample was masked off using Kapton tape to ensure the glass remained clean. Immediately prior to depositing in the IZO, the dielectric was cleaned for 2 min using a 200 W, 200 sccm oxygen plasma. This activates the surface of the HfO$_2$ and ensures good wetting of the IZO sol-gel. The IZO sol-gel was then spin-coated onto the dielectric using a static dispense through a 0.3 μm PTFR filter and was then ramped to 3000 RPM and spun for 30 s. The sample was transferred to a hotplate and baked at 150 °C for 5 min to remove excess solvent. This spin-coating process was repeated to yield a two-layer film (12–15 nm). After spin coating, the device was cured in a Sentro Tech programmable tube furnace. The sample was ramped from room temperature to 350 °C over 90 min and then held at 350 °C for 60 min. The sample was allowed to cool gradually to room temperature. After thermal processing, the semiconductor island was patterned using a photoresist and then etched in a 5:1 mixture of DI: HCl for 10 s. The source/drain electrodes were then formed by lift-off of 100 nm of aluminum deposited by e-beam evaporation. This formed a channel with a W/L ratio of 500/60 μm. Finally, a gate contact hole was opened by patterning and etching the HfO$_2$ dielectric in the ion mill.

Photonic lift-off tool

Samples were photonically lifted off using a NovaCentrix PulseForge® 1300® or a NovaCentrix PulseForge Invent (IX2-956), each equipped with a 24 mm diameter flashlamp (xenon gas-filled with beam size 150 mm × 75 mm) that emits broadband light (200–1100 nm). 1300 was equipped with four lamp drivers and a 5 kW power supply, while the Invent had five lamp drivers and a 6 kW power supply. A National Institute of Standards

and Technology (NIST)-traceable bolometer was used to measure the radiant exposure of each pulse used to lift-off the samples and calibrate the simulated temperature. The bolometer ensures that consistent processing conditions can be used in each experiment, even across multiple tools. Samples are suspended above the graphite chuck on glass slides, and the sample table height is adjusted 10 mm below the lamp housing. All PLO processing was carried out in an ambient environment.

Device characterization

TFT device characterization was accomplished using a Keysight B1500 semiconductor device parameter analyzer. Transfer curves and output curves were measured using a forward sweep followed by a reverse sweep of the gate or drain voltage, respectively. Field-effect mobility in the linear (low-field) region was calculated using the transconductance method. The device is operated in the linear region ($V_D = 0.1$ V), and the linear drain current is differentiated with respect to the gate voltage to obtain the transconductance, g_m. The oxide capacitance, C_{ox}, was measured using Mo/HfO$_2$/Al capacitors in which the HfO$_2$ was deposited using conditions identical to those used in TFT fabrication. The capacitance was measured with a gate voltage of 5 volts and a frequency of 100 Hz, yielding a capacitance of $C_{ox} = 337$ nF/cm^2. The linear mobility is then extracted using Eq. (2).

$$\mu_{FE} = \frac{L g_m}{W C_{ox} V_D} \tag{2}$$

The subthreshold slope was calculated by reciprocating the slope of the I_D-V_G transfer curve in the turn-on ($V_{ON} < V_G < V_t$) region. This was plotted against log (I_D) and the minimum subthreshold slope was taken from each curve. The TFT turn-on point (V_{ON}) is identified as the point on the transfer curve where the current abruptly increases, indicating charge accumulation in the channel. Hysteresis is defined as the difference in V_{ON} between the forward and reverse sweep of the transfer curve measured in saturation. The subthreshold slope was calculated and plotted against the drain current. This method allows to easily exclude any gate current that might contribute to errors in the subthreshold swing.

Finite element analysis (FEA) of the PLO process

The 3D FEM model geometry replicated the experimental PLO samples. This consisted of three solids representing the glass, LAL, and polyimide. The incident energy was modeled using the deposited beam power module incident on the LAL with a pulse width defined by an analytic equation and energy density determined by bolometry measurements. To capture the abrupt change in applied energy density during the short PLO pulse, an explicit event was triggered at the falling edge of the pulse width. The sample suspension during PLO was modeled by defining a convective heat flux on the external boundaries with a convective heat transfer coefficient of 15 Wm^{-2}K^{-1}. A swept mesh was applied to all geometries. A mesh distribution was applied to the glass and PI to ensure there was a denser mesh near the LAL/PI and LAL/glass interfaces.

REFERENCES

1. Khan, S., Lorenzelli, L. & Dahiya, R. S. Technologies for printing sensors and electronics over large flexible substrates: a review. *IEEE Sens. J.* **15**, 3164–3185 (2015).
2. Burns, S. Flexible displays made with plastic electronics. *Inform. Disp.* **26**, 16–19 (2010).
3. Steudel, S. et al. Design and realization of a flexible QQVGA AMOLED display with organic TFTs. *Org. Electron.* **13**, 1729–1735 (2012).
4. Yakimets, I. et al. Polymer substrates for flexible electronics: achievements and challenges. *Adv. Mat. Res.* **93–94**, 5–8 (2010).
5. Jain, K., Klosner, M., Zemel, M. & Raghunandan, S. Flexible electronics and displays: high-resolution, roll-to-roll, projection lithography and photoablation processing technologies for high-throughput production. *Proc. IEEE* **93**, 1500–1510 (2005).
6. Carlson, A., Bowen, A. M., Huang, Y., Nuzzo, R. G. & Rogers, J. A. Transfer printing techniques for materials assembly and micro/nanodevice fabrication. *Adv. Mater.* **24**, 5284–5318 (2012).
7. Bian, J. et al. Experimental study of laser lift-off of ultra-thin polyimide film for flexible electronics. *Sci. China Technol. Sci.* **62**, 233–242 (2019).
8. Delmdahl, R., Fricke, M. & Fechner, B. Laser lift-off systems for flexible-display production. *J. Inf. Disp.* **15**, 1–4 (2014).
9. Kim, Y., Noh, Y., Park, S., Kim, B.-K. & June Kim, H. Ablation of polyimide thin-film on carrier glass using 355 nm and 37 ns laser pulses. *Int. J. Heat. Mass Transf.* **147**, 118896 (2020).
10. Do, Y. H., Kang, M. G., Kim, J. S., Kang, C. Y. & Yoon, S. J. Fabrication of flexible device based on PAN-PZT thin films by laser lift-off process. *Sens. Actuators, A* **184**, 124–127 (2012).
11. Do, Y. H., Jung, W. S., Kang, M. G., Kang, C. Y. & Yoon, S. J. Preparation on transparent flexible piezoelectric energy harvester based on PZT films by laser lift-off process. *Sens. Actuators, A* **200**, 51–55 (2013).
12. Zhu, C., Guo, D., Ye, D., Jiang, S. & Huang, Y. Flexible PZT-integrated, bilateral sensors via transfer-free laser lift-off for multimodal measurements. *ACS Appl. Mater. Interfaces* **12**, 37354–37362 (2020).
13. Lee, C. H. et al. Use of laser lift-off for flexible device applications. *J. Appl. Phys.* **108**, 102814 (2010).
14. Bian, J., Zhou, L., Yang, B., Yin, Z. & Huang, Y. Theoretical and experimental studies of laser lift-off of nonwrinkled ultrathin polyimide film for flexible electronics. *Appl. Surf. Sci.* **499**, 143910 (2020).
15. Kim, Y., Park, S., Kim, B.-K., Park, W.-J. & Kim, H. J. Laser lift-off of polyimide thin-film from glass carrier using DPSS laser pulses of top-hat square profiles. *Opt. Laser Technol.* **142**, 107245 (2021).
16. Kim, K., Kim, S. Y. & Lee, J.-L. Flexible organic light-emitting diodes using a laser lift-off method. *J. Mater. Chem. C.* **2**, 2144 (2014).
17. Delmdahl, R., Pätzel, R. & Brune, J. Large-area laser-lift-off processing in micro-electronics. *Phys. Procedia* **41**, 241–248 (2013).
18. Dyer, P. E. Excimer laser polymer ablation: twenty years on. *Appl. Phys. A* **77**, 167–173 (2003).
19. Urech, L., Lippert, T., Phipps, C. R. & Wokaun, A. Polymer ablation: from fundamentals of polymer design to laser plasma thruster. *Appl. Surf. Sci.* **253**, 6409–6415 (2007).
20. Lippert, T. In *Polymers and Light* (Springer, 2004).
21. Cozzens, R. F. & Fox, R. B. Infrared laser ablation of polymers. *Polym. Eng. Sci.* **18**, 900–904 (1978).
22. Du, Q., Chen, T., Liu, J. & Zeng, X. Surface microstructure and chemistry of polyimide by single pulse ablation of picosecond laser. *Appl. Surf. Sci.* **434**, 588–595 (2018).
23. Himmelbauer, M., Arenholz, E. & Bäuerle, D. Single-shot UV-laser ablation of polyimide with variable pulse lengths. *Appl. Phys. A* **63**, 87–90 (1996).
24. Gordon, P., Balogh, B. & Sinkovics, B. Thermal simulation of UV laser ablation of polyimide. *Microelectron. Reliab.* **47**, 347–353 (2007).
25. Srinivasan, R. & Braren, B. Ultraviolet laser ablation of organic polymers. *Chem. Rev.* **89**, 1303–1316 (1989).
26. Bityurin, N., Luk'yanchuk, B. S., Hong, M. H. & Chong, T. C. Models for laser ablation of polymers. *Chem. Rev.* **103**, 519–552 (2003).
27. Kim, S. J. et al. High-performance flexible thermoelectric power generator using laser multiscanning lift-off process. *ACS Nano* **10**, 10851–10857 (2016).
28. Haq, J., Vogt, B. D., Raupp, G. B. & Loy, D. Impact of adhesive rheology on stress-distortion of bonded plastic substrates for flexible electronics applications. *Microelectron. Eng.* **88**, 2852–2856 (2011).
29. Xue, X., Yang, S. & Wang, Z. Heat-depolymerizable polypropylene carbonate as a temporary bonding adhesive for fabrication of flexible silicon sensor chips. *IEEE Trans. Compon. Packag. Manuf. Technol.* **7**, 1751–1758 (2017).
30. Haq, J., Ageno, S., Raupp, G. B., Vogt, B. D. & Loy, D. Temporary bond-debond process for manufacture of flexible electronics: impact of adhesive and carrier properties on performance. *J. Appl. Phys.* **108**, 114917 (2010).
31. Xiao, S. Y., Che, L. F., Li, X. X. & Wang, Y. L. A novel fabrication process of MEMS devices on polyimide flexible substrates. *Microelectron. Eng.* **85**, 452–457 (2008).
32. Coutts, G. M., Mansour, R. R. & Chaudhuri, S. K. A MEMS-tunable frequency-selective surface monolithically integrated on a flexible substrate. In *2007 IEEE/ MTT-S International Microwave Symposium* 497–500 (IEEE, 2007).
33. Lee, S. et al. Rigid substrate process to achieve high mobility in graphene field-effect transistors on a flexible substrate. *Carbon* **68**, 791–797 (2014).
34. Dragoi, V., Glinsner, T., Mittendorfer, G., Wimplinger, M. & Lindner, P. Reversible wafer bonding for reliable compound semiconductor processing. In *Proc. International Semiconductor Conference* 331–334 (IEEE, 2002).
35. Puligadda, R. et al. High-performance temporary adhesives for wafer bonding applications. *Mater. Res. Soc. Symp. Proc.* **970**, 409 (2006).
36. Labroo, P. & Cui, Y. Flexible graphene bio-nanosensor for lactate. *Biosens. Bioelectron.* **41**, 852–856 (2013).
37. Chi, C.-Y. et al. Heat-resistance study of thermal release tape. In *2013 8th International Microsystems, Packaging, Assembly and Circuits Technology Conference (IMPACT)* 35–38 (IEEE, 2013).
38. Ahmed, M. & Butler, D. P. Flexible substrate and release layer for flexible MEMS devices. *J. Vac. Sci. Technol. B* **31**, 050602 (2013).
39. Pecora, A. et al. Low-temperature polysilicon thin film transistors on polyimide substrates for electronics on plastic. *Solid State Electron* **52**, 348–352 (2008).
40. Yang, F. et al. Low-voltage organic single-crystal field-effect transistor with steep subthreshold slope. *ACS Appl. Mater. Interfaces* **10**, 25871–25877 (2018).
41. Idojiri, S. et al. Transfer technology using inorganic separation layer and apparatus for fabricating flexible OLED displays: technology and apparatus for flexible displays. *J. Soc. Inf. Disp.* **23**, 543–552 (2015).
42. Ko, M.-V. et al. 10.4L: late-news paper: joule heating induced lift-off technology for large area flexible AMOLED displays. *SID Symp . Dig. Tech. Pap.* **42**, 118–120 (2011).
43. Hendriks, R. & Schroder, K. A. Method for performing delamination of a polymer film. US patent 10,011,104 (2018).
44. Lee, S. I. et al. Xenon flash lamp lift-off technology without laser for flexible electronics. *Micromachines* **11**, 953 (2020).
45. Jang, S. H. et al. Investigation of the chemical structure of ultra-thin polyimide substrate for the xenon flash lamp lift-off technology. *Polymers* **13**, 546 (2021).
46. Liu, W., Turkani, V. S., Akhavan, V. & Korgel, B. A. Photonic lift-off process to fabricate ultrathin flexible solar cells. *ACS Appl. Mater. Interfaces* **13**, 44549–44555 (2021).
47. Weidling, A. M., Turkani, V. S., Luo, B., Schroder, K. A. & Swisher, S. L. Photonic curing of solution-processed oxide semiconductors with efficient gate absorbers and minimal substrate heating for high-performance thin-film transistors. *ACS Omega* **6**, 17323–17334 (2021).

AUTHOR CONTRIBUTIONS

A.M.W. and S.L.S. designed the devices. A.M.W. fabricated and characterized devices; developed the 3D simulation model; analyzed simulation and device data; and performed photonic lift-off. V.S.T. and V.A. provided guidance on PLO design and performed lift-off. K.A.S and S.L.S supervised the research and contributed to data analysis. All authors assisted with the preparation of the manuscript.

COMPETING INTERESTS

The authors declare the following competing financial interests: In accordance with our ethical obligations, the authors report that V.S.T, V.A. and K.A.S. were employed by NovaCentrix while engaged in this research project.

ADDITIONAL INFORMATION

Supplementary information The online version contains supplementary material available at https://doi.org/10.1038/s41528-022-00145-z.

Correspondence and requests for materials should be addressed to Kurt A. Schroder or Sarah L. Swisher.